Kármán street-boundary layer interactions in turbulent flow

Raphael C. O. S. Ribeiro, Ellen K. Longmire, Melissa A. Green

Aerospace Engineering and Mechanics, University of Minnesota, USA
*Corresponding author: ribei055@umn.edu

Keywords: Turbulent boundary layer, Vortex shedding, PIV

ABSTRACT

Understanding the intricate interplay between turbulent boundary layers and wake structures caused by obstacles in the flow is key to assessing the local shear stress fields as well as the drag. These types of flows can be relevant to natural phenomena including sediment and nutrient transport. While existing literature predominantly explores the flow downstream of cylinders mounted perpendicular to bounding surfaces or downstream of cylinders positioned outside the boundary layer region, this work experimentally studies the turbulent boundary layer passing over a cylindrical obstacle positioned near and parallel to the surface of an underlying solid wall. Planar particle image velocimetry (PIV) was performed in an open recirculating water channel for three test cases at a friction Reynolds number $Re_\tau = 1320$. Key parameters investigated include the cylinder diameter relative to the boundary layer thickness ($D/\delta = 0.09$ and 0.01) and the gap between the cylinder and the wall ($G/\delta = 0.09$), where the range of D/δ used is smaller than most examples found in the literature. Instantaneous and averaged velocity and vorticity fields are examined based on the PIV measurements. The results show how Kármán vortex streets and turbulent boundary layer structures interact to form unique flow features. The larger cylinder generated a clear separation downstream of its axis as well as a wake that remained coherent over a distance δ downstream. The smaller cylinder with $D/\delta = 0.01$ generated a much narrower and weaker wake but still showed a clear influence on time-averaged velocity profile. Future experiments will evaluate flow conditions further downstream as well as additional values of G/δ for the same D/δ values.

1. Introduction

Objects immersed within a turbulent boundary layer disturb the existing flow structures and often create additional ones, leading to different flow interactions. These interactions can impact sediment and nutrient transport, the scale of the turbulence, and the shear stress near boundaries like the seafloor or base of a river. Studies on flow downstream of cylinders mounted in cross-flow above a bounding surface are fairly common in the literature (e.g. Goldstein & Karni (1984), Yang & Nepf (2019), and Essel et al. (2021)). Bearman & Zdravkovich (1978) conducted an experimental investigation with relatively large cylinder diameters $D/\delta = 1.25$, where δ is the boundary layer thickness. Their focus was on the influence of the gap distance G between the wall and the cylinder on vortex shedding, and they found that the wake frequency remained constant as the gap was reduced to $G/D = 0.3$, even though the drag, base pressure, and separation position changed. By contrast, the experiments of Marumo et al. (1978) showed that the friction coefficient and the recovery rate of a turbulent boundary layer disturbed by a cylinder varied significantly with the cylinder's distance from the wall when $h/\delta < 0.222$, where h is the height of the center of the cylinder. The near-wall region recovered faster than the outer region, and the characteristics of outer-layer turbulence resembled wake turbulence with strong periodic velocity fluctuations downstream of the cylinder.

Sarkar & Sarkar (2009) performed large-eddy simulations (LES) of the flow past a circular cylinder near a flat plate for gap-to-diameter (G/D) ratios of 0.25, 0.5, and 1.0. The boundary layer upstream of the cylinder was laminar. These simulations followed the experiment of Price et al. (2002), and revealed that G/D significantly influences the wake dynamics and boundary layer evolution. The strong wake/shear layer interactions induced rapid transition of the boundary layer even at the larger gap ratios.

A more recent study by Zhou et al. (2021) et al. used particle image velocimetry (PIV) to obtain wake vector fields for $D/\delta \approx 1.5$, with G/D varying from 0 to 2.5. Using proper orthogonal decomposition (POD) on the data, different flow characteristic behaviors were classified for different values of G/D. Similar to Zhou et al. (2021), De Jesús et al. (2024) used spectral and spatial analysis to evaluate vortex shedding frequency associated with the smallest scales of the flow disturbances behind a smaller cylinder ($D/\delta = 0.05$) positioned at different gap heights in the outer region of a turbulent boundary layer. Spectral POD modes were calculated at wavelengths relevant to wake vortex shedding and energetic turbulent structures. The authors found evidence of large-scale structure suppression and augmentation of small-scale energy at and below the cylinder height. For larger gap heights, more traditional boundary layer behavior was observed with fewer apparent wake interactions.

In contrast with previous work, the current study aims to understand the effects of flow downstream of small cylinders embedded in the logarithmic region of a boundary layer. In the current study, G/δ is held constant at approximately 0.1 in a boundary layer with a constant friction Reynolds number $Re_\tau = u_\tau \delta/\nu$, where u_τ is the shear velocity and ν is the kinematic viscosity. The cylinder diameter is varied from D/δ of 0.09 down to 0.01). The overall goal is to understand the nature of the downstream evolution of the dominant wake structures and their interactions with the coherent structures in the logarithmic region.

2. Methodology

Experiments were performed in a recirculating water channel located in the Turbulent Shear Flow Laboratory in the Aerospace Engineering and Mechanics Department at the University of Minnesota. The channel test section dimensions are $7.80m \times 1.12m \times 0.58m$. The experimental setup is shown in Fig. 1. Planar PIV experiments were performed downstream of cylinders with different diameters, located at a constant gap, G, above the wall. The unperturbed flow was characterized at the same location as a base of comparison. Cylinder mounts were attached magnetically to the bottom wall $4.2m$ downstream of a tripwire located at the test section entrance. The unperturbed flow speed ($U_\infty = 0.494$ m/s) and conditions ($Re_\tau = 1320$ at cylinder location) were measured by Tee (2021) in previous work completed in the same water channel. These values were confirmed by the present study. Under these conditions, the boundary layer thickness at the cylinder location is $\delta = 70$ mm. In addition to the unperturbed condition, flow measurements were performed with D/δ of 0.01 and 0.09 at $G/\delta = 0.09$ ($G^+ = 121$).

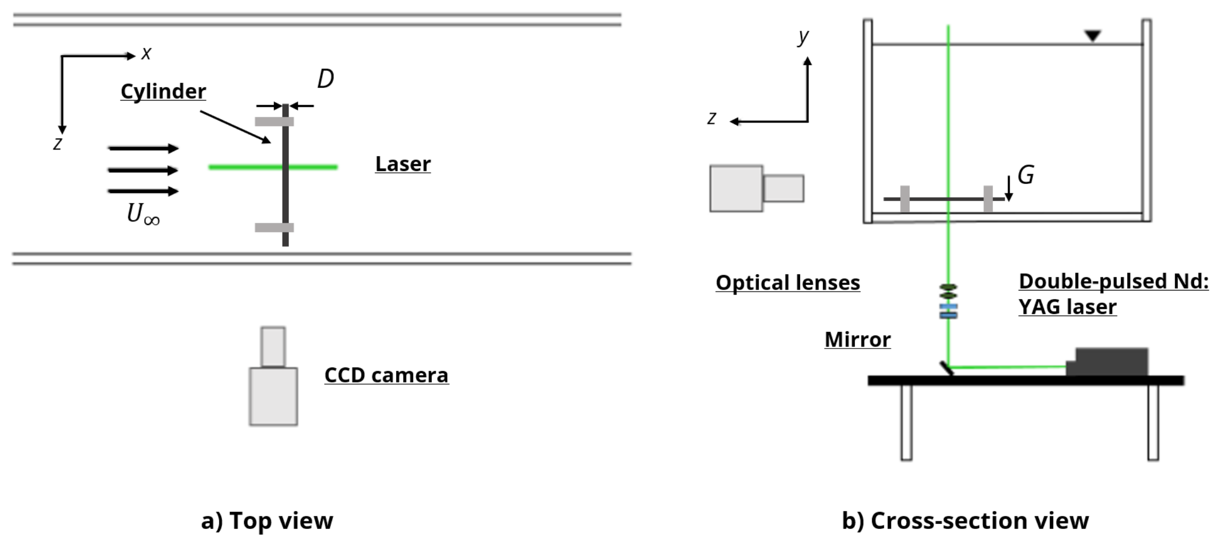

Figure 1. Experimental setup. (a) Top view: cylinder and laser sheet position within water channel. (b) Cross-section view: laser path through mirror and sheet optics.

For PIV imaging, the flow was seeded with 13μm silver-coated hollow glass spheres (Potters Industries LLC), $\rho = 1600\ kg\ m^{-3}$. Planar PIV experiments were carried out using a pair of New Wave Solo II Nd:YAG 532 nm lasers, that were attached to a TSI 610034 synchronizer box. Image pairs were captured with a TSI PowerView Plus 4MPE Camera (16-bit CCD) equipped with a Nikon AF Micro-Nikkor 105mm lens set at f/2.8. A total of 2100 image pairs were captured for each flow condition at an acquisition rate of 1 Hz. The relatively low acquisition rate was chosen to guarantee statistical independence between fields.

The PIV pre-processing included masking of the raw images and background subtraction to re-

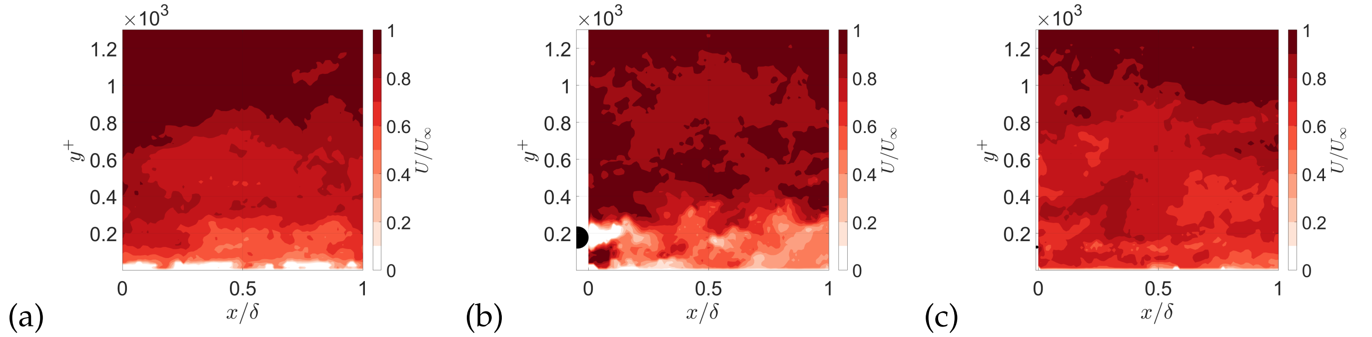

Figure 2. Instantaneous streamwise velocity fields at $Re_\tau = 1320$. (a) Unperturbed case; (b) $D/\delta = 0.09$ at $G/\delta = 0.09$; and (c) $D/\delta = 0.01$ at $G/\delta = 0.09$.

move wall reflections and enhance contrast. The image field of view after applying the mask was $\approx \delta \times \delta$ with a magnification of $46.23\ \mu m$ per pixel. Vector fields were computed using DaVis 10.4 from LaVision with a final interrogation window size of 32 by 32 pixels and an overlap of 50%. The quarter area rule (Raffel et al. (2018)) was used to determine the time between laser pulses (Δt). For an 8 pixel displacement (25% of 32), $\Delta t = 1200\ \mu s$ was selected. Averaged velocity statistics were calculated from the 2100 pairs of images obtained for each case examined.

3. Results

In Fig. 2, representative instantaneous streamwise velocity fields are shown from each case: unperturbed flow and flow behind the two cylinders, each with gap height $G/\delta = 0.09$.

In the unperturbed boundary layer (Fig. 2(a)), significant fluctuations are evident. The larger cylinder ($D/\delta = 0.09$, Fig. 2(b)) generates a clear Kármán-like wake pattern that persists through the streamwise extent of the field. Distinct perturbations are not as obvious behind the smaller cylinder ($D/\delta = 0.01$, Fig. 2(c)).

Time-averaged streamwise velocity contours are shown in Fig. 3 for the three cases. In the wake of the larger cylinder (Fig. 3(b)) there is an abrupt change in the boundary layer shape immediately downstream of the cylinder. The flow near the wall is initially accelerated, while the velocity near the cylinder axis is drastically reduced. A mean velocity deficit extends across the measurement field in x, from the wall up to $y^+ \approx 400$. The smaller cylinder (Fig. 3(c)) also alters the boundary layer profile below $y^+ \approx 400$, with both a local acceleration below its center and a velocity deficit parallel to its axis. The disturbance is clearly less pronounced compared to the large cylinder, and the flow appears to recover more quickly.

Figure 4 shows time-averaged streamwise velocity profiles at multiple streamwise positions downstream of both cylinders, scaled to the boundary layer thickness. The profile for the unperturbed case, labeled "Turbulent BL" in the legends, has the expected shape (Pope, 2000) and is included

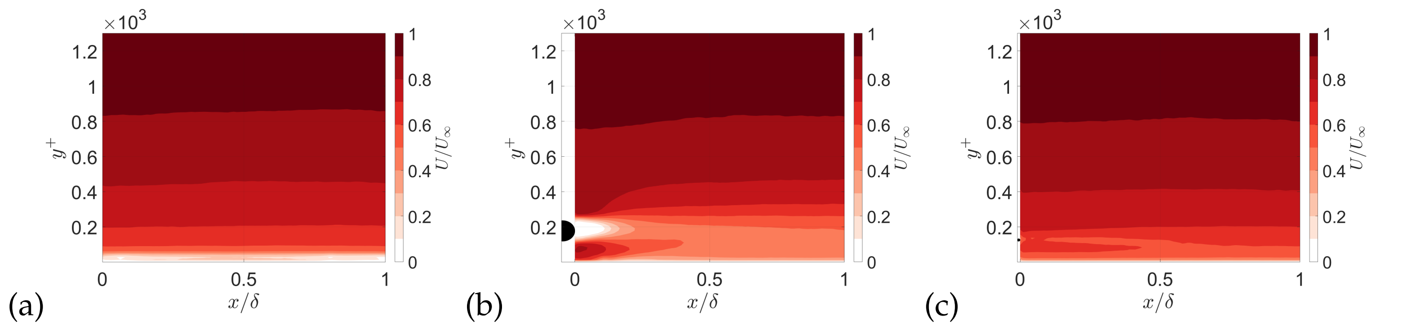

Figure 3. Time average of 2100 streamwise velocity fields for: (a) No cylinder; (b) $D/\delta = 0.09$ at $G/\delta = 0.09$; and (c) $D/\delta = 0.01$ at $G/\delta = 0.09$.

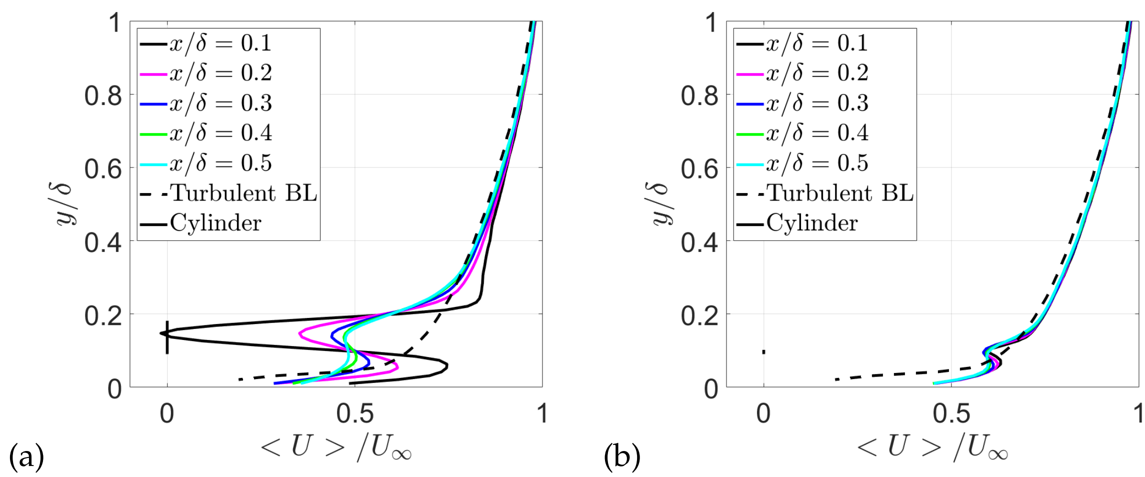

Figure 4. Streamwise time-averaged velocity profiles for (a) $D/\delta = 0.09$ and (b) $D/\delta = 0.01$.

for comparison. In both cases, the individual profiles demonstrate the zones of acceleration and deceleration compared with the unperturbed flow. The deviations from the unperturbed shape decrease gradually with downstream distance. At a given distance downstream, it is clear that the larger cylinder generates a larger magnitude deviation from the unperturbed mean profile. The mean profile downstream of the smaller cylinder, though, does not fully recover even 0.5δ downstream. While the larger cylinder generates a mean backflow that persists to $x/\delta = 0.1$, no backflow is resolved for the smaller one. The decay of the perturbations may be exhibit similarity by using the cylinder diameter as a scaling parameter instead of boundary layer thickness, and this will be considered in future work.

Non-dimensional time-averaged vorticity contours ($(dv/dx - du/dy) * \delta/U_\infty$) for the unperturbed case and in the wake of both cylinders are shown in Fig. 5. Downstream of the larger cylinder (Fig. 5(b)), the bluff body vorticity signature, with two elongated regions of negative (top) and positive (bottom) shear extending 0.4δ downstream. The wake looks asymmetric beyond this point as the negative counter-clockwise vorticity section remains visible at these contour levels beyond

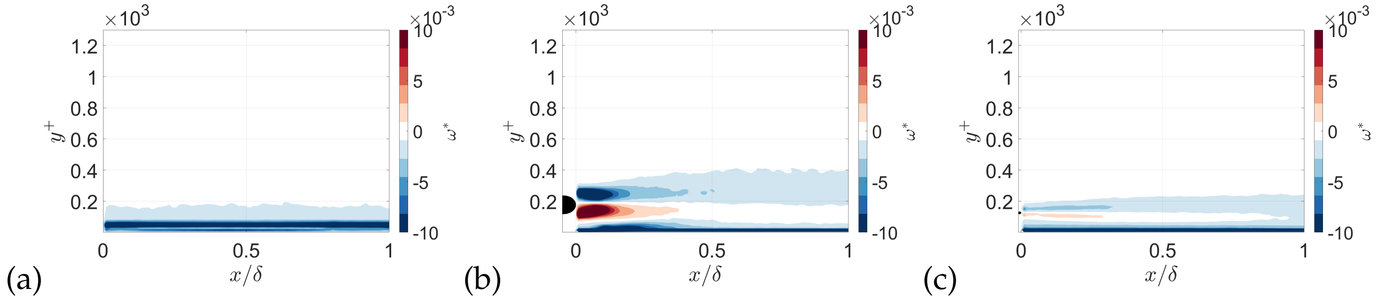

Figure 5. Time-averaged vorticity fields for (a) unperturbed flow; (b) $D/\delta = 0.09$ at $G/\delta = 0.09$ and c) $D/\delta = 0.01$ at $G/\delta = 0.09$.

the end of the data window, $\approx \delta$ while the positive clockwise section does not. Immediately downstream of the cylinder, an enlarged region of strong localized negative vorticity is present on the wall that likely results from separation there.

Similar patterns, with smaller intensity, can be observed downstream of the smaller cylinder (Fig. 5(c)). Although significantly weaker overall, the counter-clockwise (positive) vorticity between the cylinder and the gap persists to almost the same downstream distance from the cylinder, around 0.3δ, when compared to the much stronger shear layers from the larger cylinder.

Examples of instantaneous vorticity fields are provided for the three flow cases in Figs. 6 to 8. In all cases, the strong shearing near the wall yields strong clockwise (negative) vorticity there that is transported away from the wall by coherent eddies. The instantaneous fields behind the larger cylinder in Fig. 7 show the presence of a Kármán vortex street with the associated regions of alternating positive and negative vorticity extending up to $y^+ \approx 400$. It is possible to see asymmetry in the vortices shed from the top and bottom of the cylinder, most evident in Fig. 7(a) and Fig. 7(b) as the positive vortex tilts away from the wall while shedding. The two instantaneous vorticity fields in the wake of the smaller cylinder (Fig. 8) reveal a weaker, but still recognizable, von Kármán street. In addition, there are extended zones of counterclockwise vorticity in the wake near y+ 150 that are not present in the unperturbed case.

Representative contours of instantaneous wall-normal velocity fluctuations are shown in Fig. 9 to Fig. 11. The Kármán street patterns behind the larger cylinder in Fig. 10 are even more apparent than in the vorticity contours. The strong fluctuations appear to interact with the pre-existing turbulent structures, creating local increases in size and magnitude of the wall-normal fluctuations at heights up to $y^+ \approx 800$. Wall-normal velocity fluctuations associated with Kármán vortices downstream of the smaller cylinder (Fig. 11) are smaller in magnitude and only appear to persist $\approx 0.3\delta$ downstream, considerably less than for the larger cylinder. Additional analysis is needed to determine how the details of how the Kármán vortices interact with existing structures and evolve further downstream.

4. Conclusions

Experiments were performed using planar PIV to investigate the behavior of the flow downstream of cylinders immersed in the logarithmic region of a turbulent boundary layer with $Re_\tau = 1320$. Two cylinder ($D/\delta = 0.01$ and 0.09) were used with a fixed gap ($G/\delta = 0.09$) above the wall. The resulting mean and fluctuating velocity and vorticity fields allowed several observations to be made.

As expected, the larger cylinder generates a much stronger wake that persists across and beyond the streamwise extent of the PIV window. It also generates a separation zone at the wall immediately downstream of its axis. The strong wake includes a significant mean reversed flow region and a persistent vortex street. The eddies in the vortex street induce strong wall-normal motions spanning to the outer boundary layer and appear to interact with larger pre-existing boundary layer structures.

The smaller cylinder generates a narrower wake with smaller von Kármán structures that become less observable as they interact with the background turbulent boundary layer structures. The mean vorticity field, however, was also notably altered beyond the streamwise extent of the PIV window (1δ). The counter-clockwise vorticity from the wall-side wake of each cylinder suppressed the mean clockwise vorticity near the wall, and the clockwise vorticity from the outer side of the wake thickened the clockwise rotating region so that it extended further from the wall compared with the unperturbed case.

Additional studies are in progress to capture data further downstream of each cylinder and to examine more combinations of diameter-gap ratio. Furthermore, we are working on auxiliary identification tools to analyze the effects of the wake/boundary layer interactions.

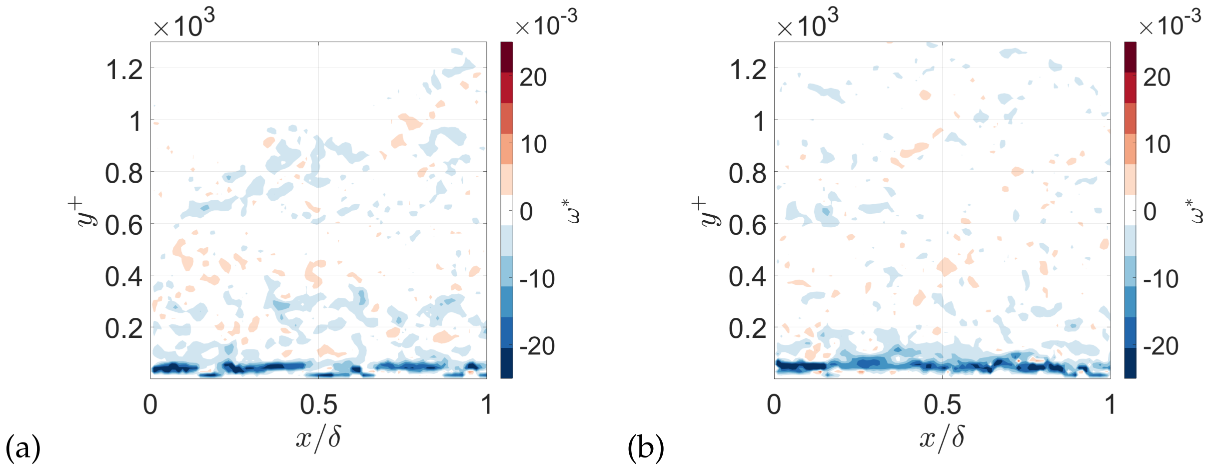

Figure 6. Instantaneous vorticity fields without cylinder.

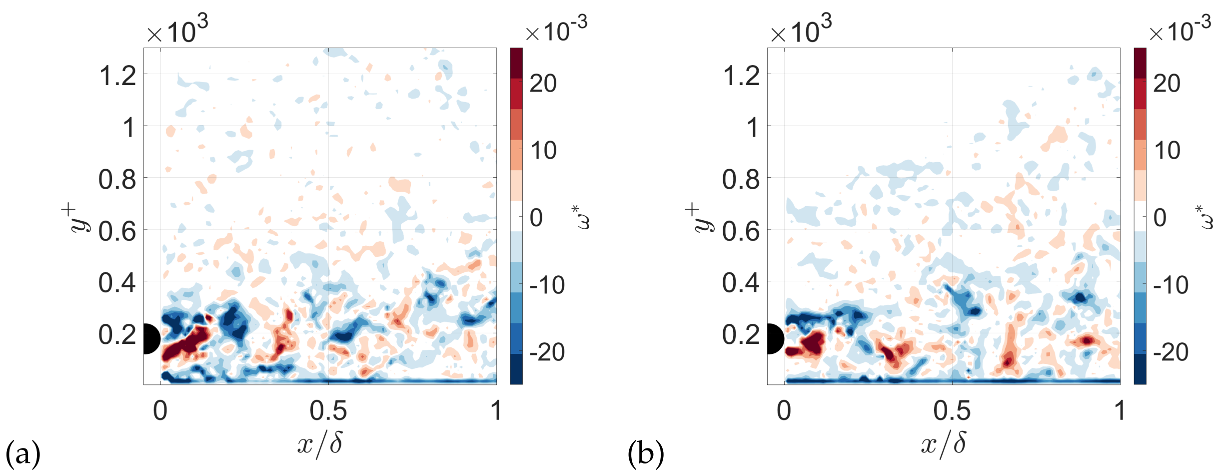

Figure 7. Instantaneous vorticity fields for $D/\delta = 0.09$ at $G/\delta = 0.09$.

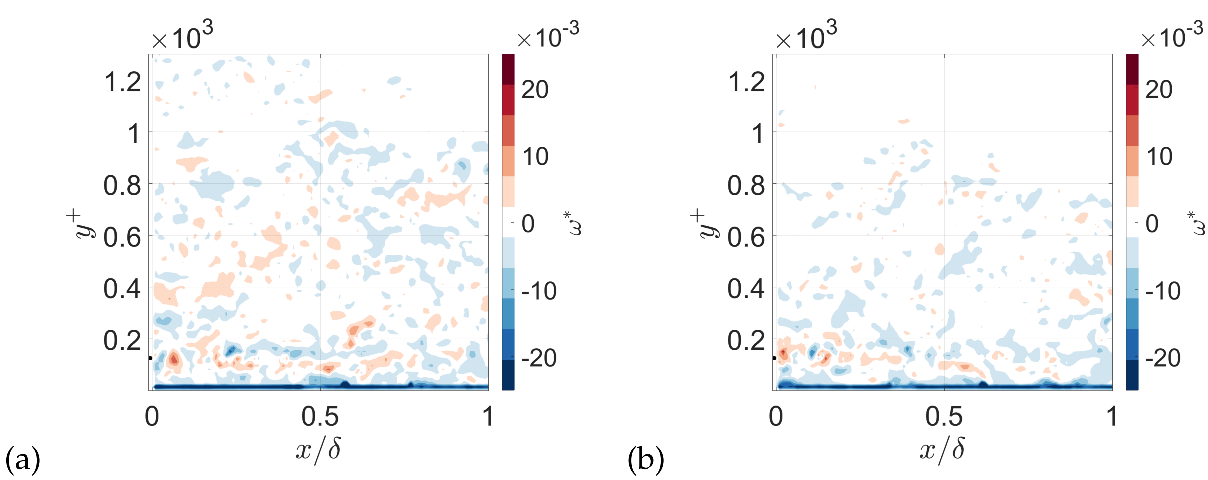

Figure 8. Instantaneous vorticity fields for $D/\delta = 0.01$ at $G/\delta = 0.09$.

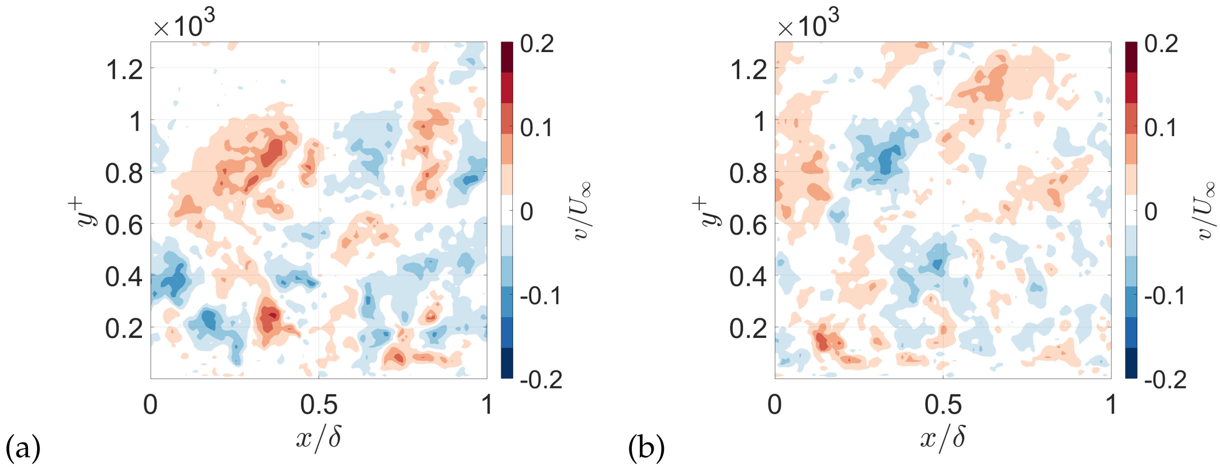

Figure 9. Instantaneous wall-normal velocity fluctuation fields for the unperturbed case.

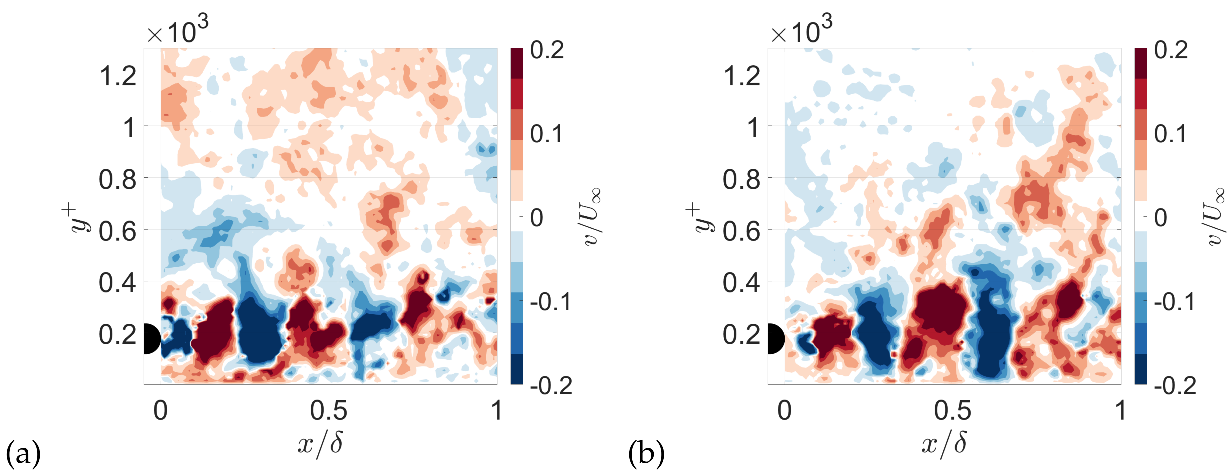

Figure 10. Instantaneous wall-normal velocity fluctuation fields for $D/\delta = 0.09$.

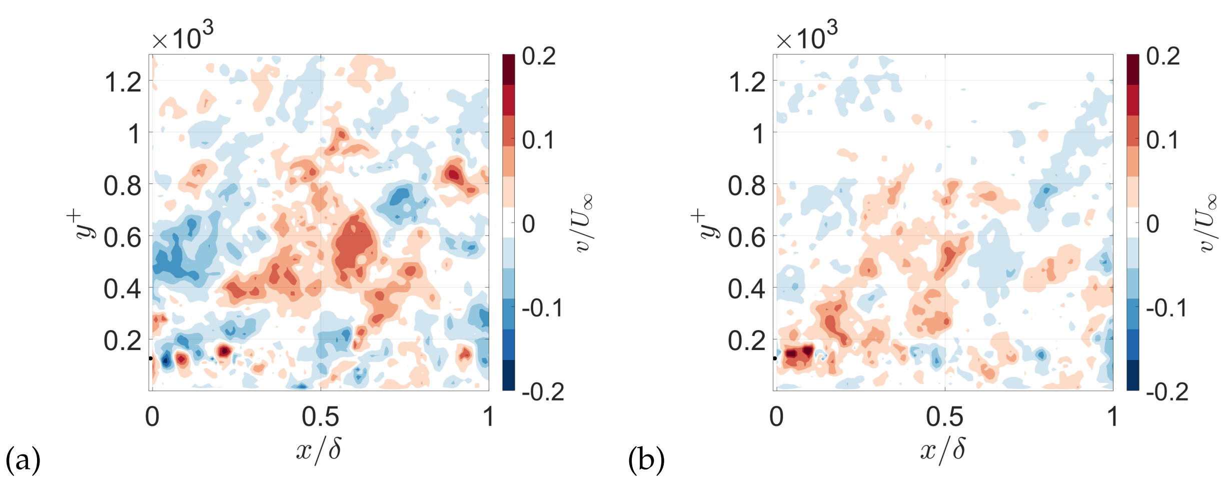

Figure 11. Instantaneous wall-normal velocity fluctuation fields for $D/\delta = 0.01$.

Acknowledgements

We wish to thank Professor Ronald J. Adrian and acknowledge the generous support of the Adrian Graduate Student Travel Award, which made it possible for the first author to attend and present our research findings at the conference.

References

Bearman, P. W., & Zdravkovich, M. M. (1978). Flow around a circular cylinder near a plane boundary. *Journal of Fluid Mechanics*, *89*(1), 33–47. doi: 10.1017/S002211207800244X

De Jesús, E. T., Waghmare, P., & Saxton-Fox, T. (2024). Spectral analysis of a cylinder wake interacting with coherent structures in a turbulent boundary layer. In *Aiaa scitech forum and exposition, 2024.*

Essel, E. E., Tachie, M. F., & Balachandar, R. (2021). Time-resolved wake dynamics of finite wall-mounted circular cylinders submerged in a turbulent boundary layer. *Journal of Fluid Mechanics*, *917*, A8. doi: 10.1017/jfm.2021.265

Goldstein, R. J., & Karni, J. (1984, 05). The Effect of a Wall Boundary Layer on Local Mass Transfer From a Cylinder in Crossflow. *Journal of Heat Transfer*, *106*(2), 260-267. Retrieved from `https://doi.org/10.1115/1.3246667` doi: 10.1115/1.3246667

Marumo, E., Suzuki, K., & Sato, T. (1978). A turbulent boundary layer disturbed by a cylinder. *Journal of Fluid Mechanics*, *87*(1), 121–141. doi: 10.1017/S0022112078002967

Pope, S. B. (2000). *Turbulent flows*. Cambridge University Press. doi: 10.1017/CBO9781316179475

Price, S., Sumner, D., Smith, J., Leong, K., & Païdoussis, M. (2002). Flow visualization around a circular cylinder near to a plane wall. *Journal of Fluids and Structures*, *16*(2), 175-191. Retrieved from `https://www.sciencedirect.com/science/article/pii/S088997460190413X` doi: https://doi.org/10.1006/jfls.2001.0413

Raffel, M., Willert, C. E., Scarano, F., Kähler, C. J., Wereley, S. T., & Kompenhans, J. (2018). *Particle image velocimetry: a practical guide*. springer.

Sarkar, S., & Sarkar, S. (2009, 08). Large-Eddy Simulation of Wake and Boundary Layer Interactions Behind a Circular Cylinder. *Journal of Fluids Engineering*, *131*(9), 091201. Retrieved from `https://doi.org/10.1115/1.3176982` doi: 10.1115/1.3176982

Tee, Y. H. (2021). *Resolving particle dynamics in turbulent wall-bounded flow* (Unpublished doctoral dissertation). UMN.

Yang, J. Q., & Nepf, H. M. (2019). Impact of vegetation on bed load transport rate and bedform characteristics. *Water Resources Research*, *55*(7), 6109-6124. doi: https://doi.org/10.1029/2018WR024404

Zhou, J., Qiu, X., Li, J., & Liu, Y. (2021, 03). The gap ratio effects on vortex evolution behind a circular cylinder placed near a wall. *Physics of Fluids*, *33*(3), 037112. doi: 10.1063/5.0039611